The Astrophysical Journal, 664:1093–1101, 2007 August 1

EXTENDED ENVELOPES AROUND GALACTIC CEPHEIDS. III. Y OPHIUCHI AND α PERSEI FROM NEAR-INFRARED INTERFEROMETRY WITH CHARA/FLUOR

Antoine Mérand
Center for High Angular Resolution Astronomy, Georgia State University, PO Box 3965, Atlanta, GA 30302-3965; antoine@chara-array.org

Jason P. Aufdenberg
Physical Sciences Department, Embry-Riddle Aeronautical University, Daytona Beach, FL 32114

Pierre Kervella and Vincent Coudé du Foresto
LESIA, UMR 8109, Observatoire de Paris, 5 place Jules Janssen, 92195 Meudon, France

and

Theo A. ten Brummelaar, Harold A. McAlister, Laszlo Sturmann, Judit Sturmann, and Nils H. Turner
Center for High Angular Resolution Astronomy, Georgia State University, PO Box 3965, Atlanta, GA 30302-3965
Received 2007 February 23; accepted 2007 April 2

ABSTRACT

Unbiased angular diameter measurements are required for accurate distances to Cepheids using the interferometric Baade-Wesselink method (IBWM). The precision of this technique is currently limited by interferometric measurements at the 1.5% level. At this level, the center-to-limb darkening (CLD) and the presence of circumstellar envelopes (CSE) seem to be the two main sources of bias. The observations we performed aim at improving our knowledge of the interferometric visibility profile of Cepheids. In particular, we assess the systematic presence of CSE around Cepheids in order determine accurate distances with the IBWM free from CSE biased angular diameters. We observed a Cepheid (Y Oph) for which the pulsation is well resolved and a nonpulsating yellow supergiant (α Per) using long-baseline near-infrared interferometry. We interpreted these data using a simple CSE model we previously developed. We found that our observations of α Per do not provide evidence for a CSE. The measured CLD is explained by an hydrostatic photospheric model. Our observations of Y Oph, when compared to smaller baseline measurements, suggest that it is surrounded by a CSE with characteristics similar to CSEs found previously around other Cepheids. We have determined the distance to Y Oph to be $d = 491 \pm 18$ pc. Additional evidence points toward the conclusion that most Cepheids are surrounded by faint CSEs, detected by near-infrared interferometry: after observing four Cepheids, all show evidence for a CSE. Our CSE nondetection around a nonpulsating supergiant in the instability strip, α Per, provides confidence in the detection technique and suggests a pulsation driven mass-loss mechanism for the Cepheids.

Subject headings: Cepheids — circumstellar matter — stars: individual (Y Ophiuchi, α Persei) — techniques: interferometric

1. INTRODUCTION

In our two previous papers, (Kervella et al. 2006; Mérand et al. 2006b, hereafter Paper I and Paper II), we reported the discovery of faint circumstellar envelops (CSEs) around Galactic classical Cepheids. Interestingly, all the Cepheids we observed (ℓ Car in Paper I, α UMi and δ Cep in Paper II) were found to harbor CSEs with similar characteristics: a CSE 3–4 times larger than the star, which accounts for a few percent of the total flux in the infrared *K* band. The presence of CSEs was discovered in our attempt to improve our knowledge of Cepheids in the context of distance determination via the interferometric Baade-Wesselink method (IBWM). Part of the method requires the measurement of the angular diameter variation of the star during its pulsation. The determination of the angular diameters from sparse interferometric measurements is not straightforward, because optical interferometers gather high angular resolution data only at a few baselines at a time; thus good phase and angular resolution coverage cannot be achieved in a short time. For Cepheids, the main uncertainty in the IBWM was thought to be the center-to-limb darkening (CLD), which biases the interferometric angular diameter measurements (Marengo et al. 2004).

The direct measurement of CLD is possible using an optical interferometer, given sufficient angular resolution and precision. Among current optical interferometers, CHARA/FLUOR (ten Brummelaar et al. 2005; Mérand et al. 2006a) is one of the few capable of such a measurement for Cepheids. The only Cepheid accessible to CHARA/FLUOR, i.e., large enough in angular diameter, for such a measurement is Polaris (α UMi), which we observed and found to have a CLD compatible with hydrostatic photospheric models, although surrounded by a CSE (Paper II). Polaris, however, is a very low-amplitude pulsation Cepheid 0.4% in diameter, compared to 15%–20% for type I Cepheids (Moskalik & Gorynya 2005); thus, the agreement is not necessarily expected for large amplitude Cepheids, whose photospheres are more out of equilibrium. The direct measurement of CLD of a high-amplitude Cepheid during its pulsation phase remains to be performed.

Hydrodynamic simulations (Marengo et al. 2003) suggest that the CLD variations during the pulsation do not account for more than a 0.2% bias in distance determination in the near-infrared using the IBWM, where most of the IBWM observing work has been done in recent years: the best formal distance determination to date using the IBWM is of the order of 1.5% (Mérand et al. 2005b).

Whereas the near-infrared IBWM seems to be relatively immune to bias from CLD, the recent discovery of CSEs raises the issue of possible bias in angular diameter measurements, and hence bias in distance estimations at the 10% level (Paper II). It

is therefore important to continue the study of CSEs around Cepheids. We present here interferometric observations of the nonpulsating supergiant α Per and the low-amplitude Cepheid Y Oph. We obtained these results in the near-infrared K band using the Fiber Linked Unit for Optical Recombination (FLUOR; Mérand et al. 2006a), installed at Georgia State University's Center for High Angular Resolution Astronomy (CHARA) Array located on Mount Wilson, California (ten Brummelaar et al. 2005).

2. THE LOW-AMPLITUDE CEPHEID Y OPH

In the General Catalog of Variable Stars (GCVS; Kholopov et al. 1998), Y Oph is classified in the DCEPS category, i.e., low-amplitude Cepheids with almost symmetrical light curves and with periods less than 7 days. The GCVS definition adds that DCEPS are first-overtone and/or crossing the instability strip for the first time. A decrease in photometric variation amplitude over time has been measured, as well as a period change (Fernie et al. 1995b). Using this period change rate, 7.2 ± 1.5 s yr^{-1} and the period of 17.1207 days, the star can be identified as crossing the instability strip for the third time according to models (Turner et al. 2006).

The fact that Y Oph belongs to the DCEPS category is questionable: its period is longer than 7 days, by almost 3 times, although its light curve is quasi-symmetric and with a low amplitude compared to other type I Cepheids of similar periods (Vinko et al. 1998). Indeed, Y Oph is almost equally referred to in publications as being a fundamental-mode Cepheid or a first overtone.

In this context, a direct determination of the linear diameter can settle whether Y Oph belongs to the fundamental mode group or not. This is of prime importance: because of its brightness and the large amount of observational data available, Y Oph is often used to calibrate the period-luminosity (PL) or the period-radius (PR) relations. The interferometric Baade-Wesselink method offers this opportunity to geometrically measure the average linear radius of pulsating stars: if Y Oph is not a fundamental pulsator, its average linear diameter should depart from the classical PR relation.

2.1. *Interferometric Observations*

The direct detection of angular diameter variations of a pulsating star has been achieved for many stars now using optical interferometers (Lane et al. 2000; Kervella et al. 2004a; Mérand et al. 2005b). We showed (Mérand et al. 2006b) that for a given average diameter, one should use a baseline that maximizes the amplification factor between the variation in angular diameter and observed squared visibility. This baseline provides an angular resolution of the order of $B\theta/\lambda \approx 1$, in other words in the first lobe, just before the first minimum ($B\theta/\lambda \approx 1.22$ for a uniform disk model), where B is the baseline (in meters), θ is the angular diameter (in radians), and λ is the wavelength of observation (in meters). According to previous interferometric measurements (Kervella et al. 2004a), the average angular diameter of Y Oph is of the order of 1.45 mas (milliarcsecond). Ideally, that would mean using a baseline of the order of 300 m, which is available at the CHARA Array. Because of a trade we made with other observing programs, we used only a 250 m baseline provided by telescopes S1 and E2.

The fringes squared visibility is estimated using the integration of the fringes power spectrum. A full description of the algorithm can be found in Coude Du Foresto et al. (1997) and Mérand et al. (2006a). The raw squared visibilities have been calibrated using resolved calibrator stars, chosen from a specific catalog (Mérand et al. 2005a) using criteria defined to minimize the calibration bias and maximize signal-to-noise ratio. The error introduced by the uncertainty on each calibrator's estimated angular diameter has been properly propagated. Among the three main calibrators (Table 1), one, HR 6639, turned out to be inconsistent with the others. The raw visibility of this star was found to vary too much to be consistent with the expected statistical dispersion. The quantity to calibrate, the interferometric efficiency (also called instrument visibility), is very stable for an instrument using single-mode fibers, such as FLUOR. If this quantity is assumed to be constant over a long period of time, and if observations of a given simple star are performed several times during this period, one can check whether or not the variation of the raw visibilities with respect to the projected baseline is consistent with a uniform disk model. Doing so, HR 6639 was found to be inconsistent with the other stars observed during the same night (Fig. 1). The inconsistency may be explained by the presence of a faint companion with a magnitude difference of 3 or 4 with respect to the primary. Two other calibrators, from another program, were also used as check stars: HR 7809 and ρ Aql (Table 1). This latter calibrator is not part of the catalog by Mérand et al. (2005a). Its angular diameter has been determined using the Kervella et al. (2004b) surface brightness calibration applied to published photometric data in the visible and near-infrared.

TABLE 1
Y Oph Calibrators

Star	Spectral Type	UD Diameter (mas)	Notes
HD 153033	K5 III	1.100 ± 0.015	
HD 175583	K2 III	1.021 ± 0.014	
HR 6639.....	K0 III	0.904 ± 0.012	rejected
HR 7809.....	K1 III	1.055 ± 0.015	
ρ Aql	A2 V	0.370 ± 0.005	not in M05

Notes.—Uniform disk diameters, given in mas, are only intended for computing the expected squared visibility in the K band. All stars but ρ Aql are from M05 catalog (Mérand et al. 2005a). Refer to text for an explanation why HR 6639 has been rejected.

For each night we observed Y Oph, we determined a uniform disk (UD) diameter (Table 2) based on several squared visibility measurements (Table 3). Each night was assigned a unique pulsation phase established using the average date of observation and the Fernie et al. (1995b) ephemeris, including the measured period change:

$$D = \mathrm{JD} - 2440007.720, \quad (1)$$

$$E = 0.05839D - 3.865 \times 10^{-10} D^2, \quad (2)$$

$$P = 17.12507 + 3.88 \times 10^{-6} E, \quad (3)$$

where E is the epoch of maximum light (the fractional part is the pulsation phase), and P is the period at this epoch.

2.2. *Pulsation*

2.2.1. *Radial Velocity Integration*

In order to measure the distance to a pulsating star, the IBWM makes use of radial velocities and angular diameters. The latter is the integral other time of the former. The radial velocities, which have been acquired at irregular intervals during the pulsation phase, must be numerically integrated. This process is highly sensitive to noisy data, and the best way to achieve a robust integration is to interpolate the data before integration. For this purpose, we use a periodic cubic spline function, defined by floating nodes

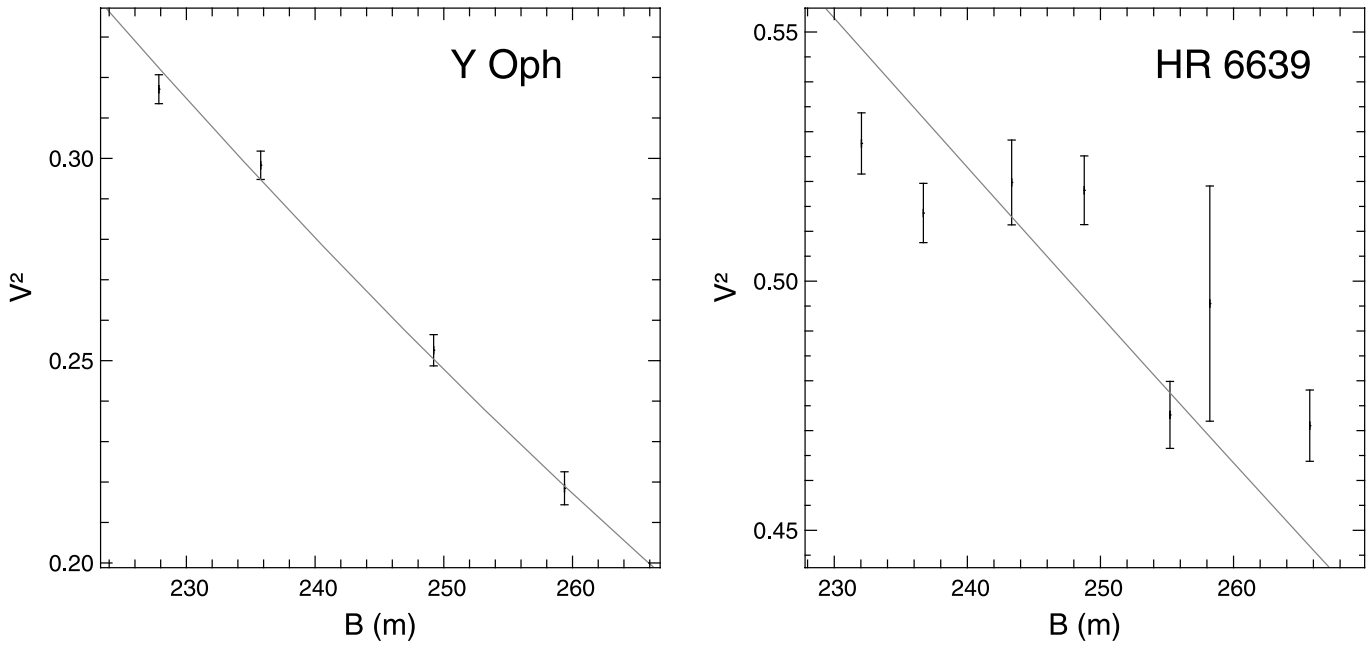

FIG. 1.—Evidence that calibrator HR 6639 is probably a binary star. Calibrated squared visibility as a function of baseline for UT 2006 July 10. Left is Y Oph, and right is HR 6639. The interferometric efficiency was supposed constant during the night and established using HR 7809 and ρ Aql with a reduced χ^2 of 1.3. A UD fit, shown as a continuous line, works for Y Oph ($\chi^2_r = 0.6$), whereas it fails for HR 6639 ($\chi^2_r = 7.2$). This could be the sign that HR 6639 has a faint companion: the visibility variation has a 3%–5% amplitude, which corresponds to a magnitude difference of 3–4 between the main star and its companion.

(Fig. 2). The coordinates of these nodes are adjusted such that the cubic spline function going through these nodes provides the best fit to the data points. The phase positions ϕ_i of these nodes are forced to be between 0 and 1, but they are replicated every $\phi_i + n$, where n is an integer, in order to obtain a periodic function of period 1.

Among published Y Oph radial velocities data, we chose Gorynya et al. (1998) because of the uniform phase coverage and the algorithm used to extract radial velocities: the cross-correlation method. As shown by Nardetto et al. (2004), the method used can influence the distance determination via the choice of the so-called projection factor, which we shall introduce in § 2.2.2. The pulsation phases have been also determined using equation (2).

The data presented by Gorynya et al. (1998) were acquired between 1996 June and 1997 August. As we already mentioned, Y Oph is known for its changing period and photometric amplitude.

TABLE 2
Y OPH ANGULAR DIAMETERS

MJD−53,900	ϕ	N_{obs}	B (m)	θ_{UD} (mas)	χ^2
18.292.....	0.248	3	207–230	1.3912 ± 0.0067	0.55
21.279.....	0.423	3	208–233	1.3516 ± 0.0074	1.06
22.232.....	0.478	3	229–246	1.3387 ± 0.0077	0.05
24.210.....	0.594	3	235–254	1.2929 ± 0.0059	0.19
26.207.....	0.710	4	228–259	1.2488 ± 0.0029	0.61
27.221.....	0.770	4	223–248	1.2374 ± 0.0032	0.76
28.249.....	0.830	2	219–226	1.2394 ± 0.0055	0.30
29.237.....	0.887	3	220–234	1.2728 ± 0.0047	0.26
30.229.....	0.945	5	216–245	1.2715 ± 0.0030	0.56

NOTES.—Data points have been reduced to one uniform disk diameter per night. Avgerage date of observation (Modified Julian Day), pulsation phase, number of calibrated V^2, projected baseline range, uniform disk angular diameter, and reduced χ^2.

TABLE 3
JOURNAL OF OBSERVATIONS: Y OPH

MJD−53,900	B (m)	P.A. (deg)	V^2
18.260.....	229.808	63.540	0.2348 ± 0.0061
18.296.....	215.049	71.242	0.2823 ± 0.0065
18.321.....	207.247	77.913	0.3030 ± 0.0075
21.245.....	232.792	62.353	0.2511 ± 0.0065
21.283.....	216.576	70.243	0.2954 ± 0.0085
21.309.....	208.313	76.765	0.3194 ± 0.0085
22.212.....	245.894	58.023	0.2092 ± 0.0071
22.234.....	236.338	61.050	0.2352 ± 0.0078
22.251.....	228.941	63.902	0.2615 ± 0.0085
24.188.....	253.988	55.914	0.2108 ± 0.0062
24.212.....	243.641	58.680	0.2427 ± 0.0060
24.231.....	235.388	61.389	0.2634 ± 0.0065
26.168.....	259.377	54.714	0.2185 ± 0.0041
26.194.....	249.210	57.113	0.2526 ± 0.0039
26.224.....	235.772	61.251	0.2983 ± 0.0034
26.242.....	227.859	64.367	0.3171 ± 0.0035
27.194.....	247.788	57.495	0.2650 ± 0.0040
27.211.....	240.340	59.704	0.2854 ± 0.0038
27.228.....	232.806	62.348	0.3177 ± 0.0045
27.250.....	223.415	66.429	0.3385 ± 0.0045
28.241.....	225.978	65.207	0.3332 ± 0.0045
28.257.....	219.413	68.547	0.3629 ± 0.0061
29.219.....	234.329	61.775	0.2857 ± 0.0049
29.237.....	226.405	65.012	0.3148 ± 0.0053
29.253.....	219.709	68.380	0.3320 ± 0.0054
30.192.....	245.267	58.203	0.2510 ± 0.0035
30.216.....	234.738	61.624	0.2893 ± 0.0041
30.235.....	226.418	65.007	0.3112 ± 0.0044
30.244.....	222.544	66.866	0.3226 ± 0.0046
30.261.....	215.937	70.653	0.3462 ± 0.0048

NOTE.—Date of observation (Modified Julian Day), telescope projected separation (m), baseline projection angle (degrees), and squared visibility.

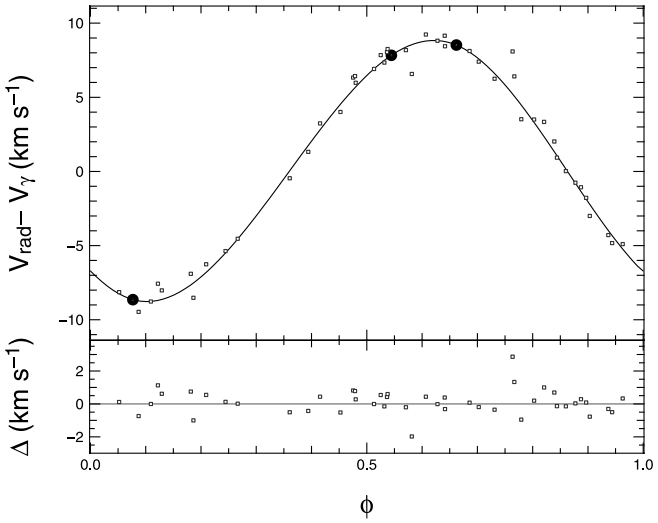

FIG. 2.—Y Oph radial velocities from Gorynya et al. (1998). The continuous line is the periodic spline function defined by three adjustable floating nodes (*large filled circles*). The systematic velocity, $V_\gamma = -7.9 \pm 0.1$ km s^{-1}, has been evaluated using the interpolation function and removed. The lower panel displays the residuals of the fit.

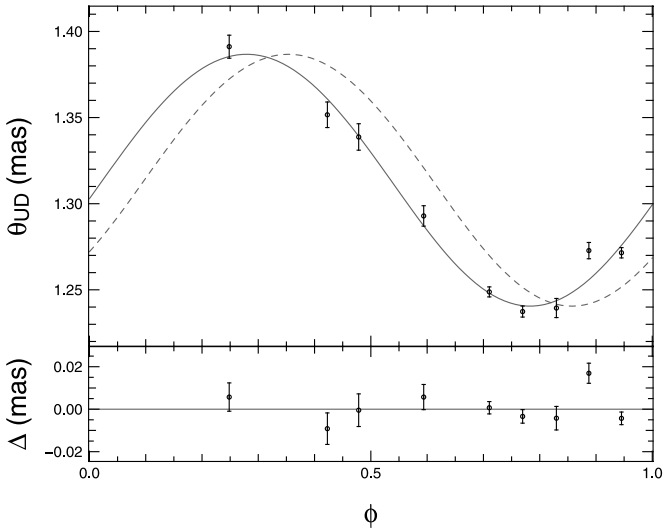

FIG. 3.—Y Oph angular diameter variations. Upper panel shows CHARA/FLUOR uniform disk angular diameters as a function of phase. Each data point corresponds to a given night, which contains several individual squared visibility measurements (Table 2). The solid line is the integration of the radial velocity (Fig. 2) with distance, average angular diameter, and phase shift adjusted. The dashed line has a phase shift set to zero. The lower panel shows the residuals to the continuous line.

Based on Fernie et al. (1995b), the decrease in amplitude observed for the photometric B and V bands does not have a measurable counterpart in radial velocity. This is why we did not apply any correction in amplitude to the radial velocity data in order to take into account the 10 years between the spectroscopic and interferometric measurements.

2.2.2. *Distance Determination Method*

Once radial velocities $v_{\rm rad}$ are interpolated (Fig. 2) and integrated, the distance d is determined by fitting the radial displacement to the measured angular diameters (Fig. 3)

$$\theta_{\rm UD}(T) - \theta_{\rm UD}(0) = -2\frac{kp}{d}\int_0^T v_{\rm rad}(t)\,dt, \qquad (4)$$

where $\theta_{\rm UD}$ is the interferometric uniform disk diameter, and k is defined as the ratio between $\theta_{\rm UD}$ and the true stellar angular diameter. The projection factor, p, is the ratio between the pulsation velocity and the spectroscopically measured radial velocity. The actual parameters of the fit are the average angular diameter $\theta_{\rm UD}(0)$ and the biased distance d/kp.

This formalism assumes that neither k or p vary during the pulsation. There is evidence that this might be true for k, based on hydrodynamic simulation (Marengo et al. 2003) at the 0.2% level. Observational evidence exists as well: when we measured the p-factor of δ Cep (Mérand et al. 2005b), we did not find any difference between the shapes of the left and right parts of equation (4); therefore kp is probably constant over a pulsation period, at least at the level of precision we have available.

For this work, we will adopt the value for p we determined observationally for near-infrared interferometry/cross-correlation radial velocity: $p = 1.27$. This result has been established for δ Cep (Mérand et al. 2005b). This is also the latest value computed from hydrodynamical photospheric models (Nardetto et al. 2004). The IBWM fit yields a biased distance $d/k = 480 \pm 18$ pc and an average angular uniform disk diameter $\theta_{\rm UD}(0) = 1.314 \pm 0.005$ mas. Note that we had to allow a phase shift between interferometric and radial velocity observations of -0.074 ± 0.005 (Fig. 3). The final reduced χ^2 is of the order of 3, mostly due to one data point ($\phi = 0.887$).

2.2.3. *Choice of k*

Usually, the choice of k is made assuming the star is a limb-darkened disk. The strength of the CLD is computed using photospheric models, then a value of k is computed. This approach is sometimes confusing because, even for a simple limb-darkened disk, there is no unique value of k, in the sense that this value varies with respect to angular resolution. The uniform disk angular size depends on which portion of the visibility curve is measured. However, it is mostly unambiguous in the first lobe of visibility, i.e., at moderate angular resolution $B\theta/\lambda \leq 1$.

However, as shown in Paper II, the presence of a faint CSE around Cepheids biases k up to 10%, particularly when the angular resolution is moderate and the star is not well resolved ($V^2 \sim 0.5$). Under these conditions, the CSE is largely resolved, leading to a strong bias if the CSE is omitted. On the other hand, at greater angular resolution ($B\theta/\lambda \sim 1$), the star is fully resolved (V^2 approaches it first null), and the bias from the CSE is minimized. In any cases, it is critical to determine whether or not Y Oph is surrounded by a CSE if an accurate distance is to be derived.

2.3. *Interferometric Evidence of a CSE around Y Oph*

We propose here to compare the uniform disk diameters obtained by VLTI/VINCI (Kervella et al. 2004a) and CHARA/FLUOR (this work). This makes sense because these two instruments are very similar. Both observe in the near-infrared K band. Moreover, both instruments observed Y Oph in the first lobe of the visibility profile, although at different baselines.

If Y Oph is truly a uniform disk, or even a limb-darkened disk, the two instruments should give similar results. That is because the star's first lobe of squared visibility is insensitive to the CLD and only dependent the on the size. Conversely, if Y Oph is surrounded by a CSE, we expect a visibility deficit at smaller baseline (VLTI/VINCI), and hence a larger apparent uniform disk diameter (see Fig. 5). This is because the CSE is fully resolved at baselines which barely resolve the star.

This is indeed the case, as seen on Figure 4; VLTI/VINCI UD diameters are larger than CHARA/FLUOR's. Even if the angular

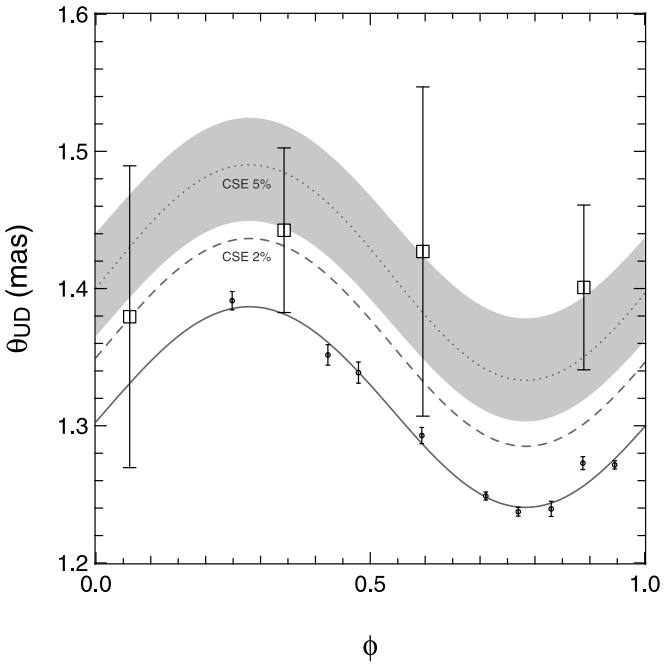

FIG. 4.—Y Oph comparison between CHARA/FLUOR and VLTI/VINCI observations. Uniform disk angular diameter as a function of phase. *Small data points* (*with small error bars*) *and lower continuous line*: CHARA/FLUOR observations and distance fit. *Large open squares*: VLTI/VINCI observations. The distance fit and its uncertainty are represented by the shaded band. *Dashed and dotted lines*: VLTI/VINCI expected biased observations based on CHARA/FLUOR and our CSE model with a flux ratio of 2% (*dashed*) and 5% (*dotted*).

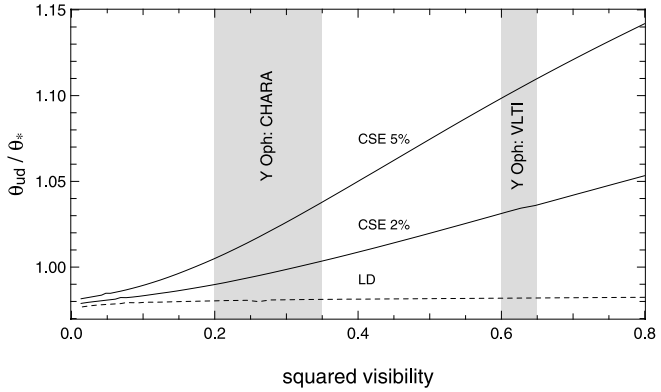

FIG. 5.—Y Oph angular diameter correction factor. We plot here $\theta_{UD}/\theta_\star$ for three different Cepheid models as a function of observed squared visibility (first lobe): the dashed line is a simple limb darkened disk with the appropriate CLD strength, and the continuous line is a similar LD disk surrounded by a CSE with a 2% *K*-band flux (short period; Polaris and δ Cep, see Paper II) and 5% (long period; ℓ Car, see Paper I). Note that, in the presence of CSE, the bias is stronger at large visibilities (hence smaller angular resolution). The shaded regions represents near infrared Y Oph observations: from CHARA (this work) and the VLTI (Kervella et al. 2004a).

resolution of VLTI/VINCI is smaller than for CHARA/FLUOR, leading to less precise angular diameter estimations, the disagreement is still statistically significant, of the order of 3 σ. Using the CSE model we can predict the correct differential UD size between the two instruments, consistent with the presence of a CSE around Y Oph. The amount of discrepancy can be used to estimate the flux ratio between the CSE and the star. In the case of Y Oph, we find that the CSE accounts for 5% $\pm$ 2% of the stellar flux. Note that for this comparison, we recomputed the phase of VLTI/VINCI data using the Fernie et al. (1995b) ephemeris presented in equation (2).

In Figure 5, we plot k as a function of the observed squared visibility for different models: hydrostatic CLD, 2% CSE, and 5% CSE (*K*-band flux ratio). For the hydrostatic model we have $k = 0.983$. For the 5% CSE models, for CHARA/FLUOR ($0.20 < V^2 < 0.35$), we have $\theta_{UD}/\theta_\star = 1.023$. This is the value we shall adopt. If we ignore the presence of the CSE, the bias introduced is $1.023/0.983 \approx 1.04$, or 4%.

2.4. *Unbiased Distance and Linear Radius*

This presence of a 5% CSE leads to an unbiased distance of $d = 491 \pm 18$ pc, which corresponds to a 3.5% uncertainty on the distance. This is to be compared with the bias we corrected for if one omits the CSE, of the order of 4%. Ignoring the CSE leads to a distance of $d = 472 \pm 18$ pc

We note that k biases only the distance, so one can form the quantity $\theta_{UD}(0)(d/k)$, which is the product of the two adjusted parameters in the fit, both biased. This quantity is by definition the linear diameter of the star and does not depend on the factor k, even if it is still biased by the choice of p. If θ is in mas and d in parsecs, then the average linear radius in solar radii is $R = 0.1075\theta d$. In the case of Y Oph, this leads to $R = 67.8 \pm 2.5\, R_\odot$.

2.5. *Conclusion*

Y Oph appears larger (over 2 σ) in the infrared *K* band at a 140 m baseline comapred to a 230 m baseline. Using a model of a star surrounded by a CSE we developed based on observations of other Cepheids, this disagreement is explained both qualitatively and quantitatively by a CSE accounting for 5% of the stellar flux in the near-infrared *K* band. This model allows us to unbias the distance estimate $d = 491 \pm 18$ pc. The linear radius estimate is not biased by the presence of CSE, and we found $R = 67.8 \pm 2.5\, R_\odot$.

Our distance is not consistent with the estimation using the Barnes-Evans method: Barnes et al. (2005) found $d = 590 \pm 42$ pc (Bayesian) and $d = 573 \pm 8$ pc (least squares). For this work, they used the same set of radial velocities we used. Our estimate is even more inconsistent with the other available interferometric estimate by Kervella et al. (2004a), $d = 690 \pm 50$ pc. This later result has been established using an hybrid version of the BW method: a value of the linear radius is estimated using the period-radius relation calibrated using classical Cepheids not measured from the data. This assumption is questionable, as we noted before, since Y Oph is a low-amplitude Cepheid. Kervella et al. (2004a) deduced $R = 100 \pm 8\, R_\odot$ from the PR relation, whereas we measured $R = 67.8 \pm 2.5\, R_\odot$. Because Y Oph's measured linear radius is not consistent with the PR relation for classical, fundamental-mode Cepheids, it is probably safe to exclude it from further calibrations. Interestingly, Barnes et al. (2005) observationally determined Y Oph's linear radius to also be slightly larger (2.5 σ) than what we find, $R = 92.1 \pm 6.6\, R_\odot$ (Bayesian) and $R = 89.5 \pm 1.2\, R_\odot$ (least squares). They use a surface brightness technique using a visible near-infrared color, such as $V-K$. This method is biased if the reddening is not well known. If the star is reddened, *V* magnitudes are increased more than *K*-band magnitudes. This leads to an underestimated surface brightness, because the star appears redder, and thus cooler than it is. The total brightness (estimated from *V*) is also underestimated. These two underestimates have opposing effects on the estimated angular diameter: an underestimated surface brightness leads to an overestimated angular diameter, whereas an underestimated luminosity leads to an underestimated angular diameter. In the case of a reddening law, the two effects combine and give rise to a

TABLE 4
JOURNAL OF OBSERVATIONS: α PER

MJD−54,000	B (m)	P.A. (deg)	V^2
46.281	147.82	79.37	0.02350 ± 0.00075
46.321	153.87	69.04	0.01368 ± 0.00067
46.347	155.79	62.17	0.01093 ± 0.00060
46.372	156.27	55.30	0.01134 ± 0.00039
46.398	155.65	48.10	0.01197 ± 0.00051
46.421	154.41	41.32	0.01367 ± 0.00052
46.442	152.94	34.84	0.01581 ± 0.00045
46.466	151.13	27.03	0.01824 ± 0.00064
46.488	149.58	19.40	0.02167 ± 0.00071
46.510	148.49	12.06	0.02250 ± 0.00058
46.539	147.77	1.53	0.02370 ± 0.00070
47.225	96.66	−44.51	0.27974 ± 0.00282
47.233	97.75	−47.34	0.27321 ± 0.00274
47.252	100.37	−53.97	0.24858 ± 0.00258
47.274	103.03	−60.91	0.23529 ± 0.00242
47.327	249.17	81.65	0.01363 ± 0.00032
47.352	251.22	74.84	0.01340 ± 0.00032
47.374	251.04	68.91	0.01330 ± 0.00035
47.380	250.67	67.10	0.01316 ± 0.00035

NOTE.—Date of observation (Modified Julian Day), telescope projected separation, baseline projection angle, and squared visibility.

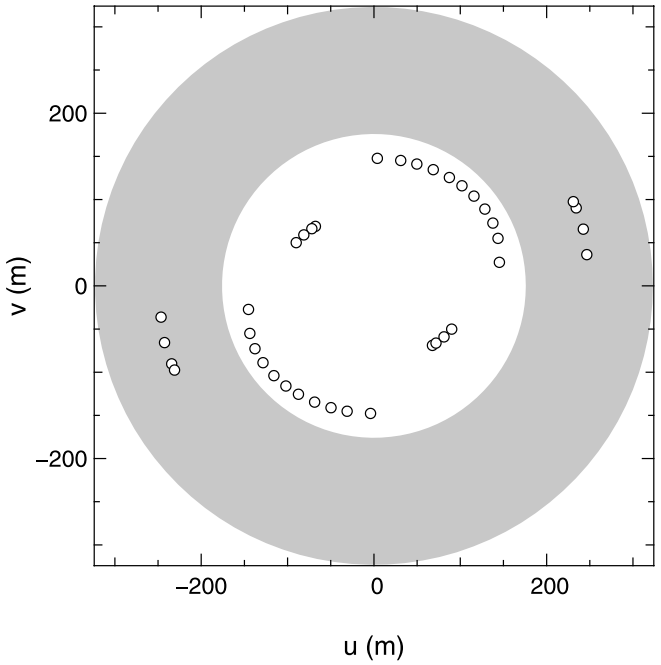

FIG. 6.—α Per. Projected baselines are in meters. North is up, and east is right. The shaded area corresponds to the squared visibility's second lobe. The baselines are W1-W2, E2-W2, and E2-W1, from the shortest to the longest.

larger angular diameter; the surface brightness effect wins over the total luminosity. Based on their angular diameter, $\theta \approx 1.45$ mas, it appears that Barnes et al. (2005) overestimated Y Oph's angular size. Among Cepheids brighter than $m_V = 6.0$, Y Oph has the strongest $B-V$ color excess, $E(B-V) = 0.645$ (Fernie et al. 1995a) and one of the highest fraction of polarized light, $p = 1.34\% \pm 0.12\%$ (Heiles 2000). Indeed, Y Oph is within the Galactic plane: this means that it has a probably a large extinction due to the interstellar medium.

3. THE NONPULSATING YELLOW SUPERGIANT α PER

α Per (HR 1017, HD 20902, F5Ib) is among the most luminous nonpulsating stars inside the Cepheids' instability strip. The Doppler velocity variability has been found to be very weak, of the order of 100 m s^{-1} in amplitude (Butler 1998). This amplitude is 10 times less than what is observed for the very low amplitude Cepheid Polaris (Hatzes & Cochran 2000).

α Per's apparent angular size, approximately 3 mas (Nordgren et al. 2001), makes it a perfect candidate for direct center-to-limb darkening detection with CHARA/FLUOR. Following the approach we used for Polaris (Paper II), we observed α Per using three different baselines, including one sampling the second lobe, in order to measure its CLD strength, but also in order to be able to assess the possible presence of a CSE around this star (Table 4).

3.1. *Interferometric Observations*

If the star is purely a CLD disk, then only two baselines are required to measure the angular diameter and the CLD strength. Observations must take place in the first lobe of the squared the visibility profile, in order to set the star's angular diameter θ. The first lobe is defined by $B\theta_{\rm UD}/\lambda < 1.22$. Additional observations should be taken in the second lobe, in particular near the local maximum ($B\theta/\lambda \sim 3/2$), because the strength of the CLD is directly linked to the height of the second lobe. To address the presence of a CSE, observations should be made at a small baseline. Because the CSEs that were found around Cepheids are roughly 3 times larger that the star itself (Papers I and II), we chose a small baseline where $B\theta/\lambda \sim 1/3$. As demonstrated by our Polaris measurements, the presence of CSE is expected to weaken the second lobe of visibility curve, mimicking stronger CLD.

FLUOR operates in the near-infrared K band with a mean wavelength of $\lambda_0 \approx 2.13$ μm. This sets the small, first-lobe and second-lobe baselines at approximately 50, 150, and 220 m, which are well matched to CHARA baselines W1-W2 (∼100 m), E2-W2 (∼150 m), and E2-W1 (∼250 m). See Figure 6 for a graphical representation of the baseline coverage.

The data reduction was performed using the same pipeline as for Y Oph. Squared visibilities were calibrated using a similar strategy we adopted for Y Oph. We used two sets of calibrators: one for the shorter baselines, W1-W2 and E2-W2, and one for the longest baseline, E2-W1 (Table 5).

3.2. *Simple Model*

3.2.1. *Limb-darkened Disk*

To probe the shape of the measured visibility profile, we first used an analytical model, which includes the stellar diameter and a CLD law. Because of its versatility, we adopt here a power law (Hestroffer 1997): $I(\mu)/I(0) = \mu^\alpha$ with $\mu = \cos(\theta)$, where θ is

TABLE 5
α PER CALIBRATORS

Name	Spectral Type	UD Diameter (mas)	Baselines
HD 18970	G9.5 III	1.551 ± 0.021	W1-W2, E2-W2
HD 20762	K0 II–III	0.881 ± 0.012	E2-W1
HD 22427	K2 III–IV	0.913 ± 0.013	E2-W1
HD 31579	K3 III	1.517 ± 0.021	W1-W2, E2-W2
HD 214995	K0 III	0.947 ± 0.013	W1-W2

NOTES.—Uniform disk diameters, given in mas, are only intended for computing the expected squared visibility in the K band. These stars come from our catalog of interferometric calibrators (Mérand et al. 2005a).

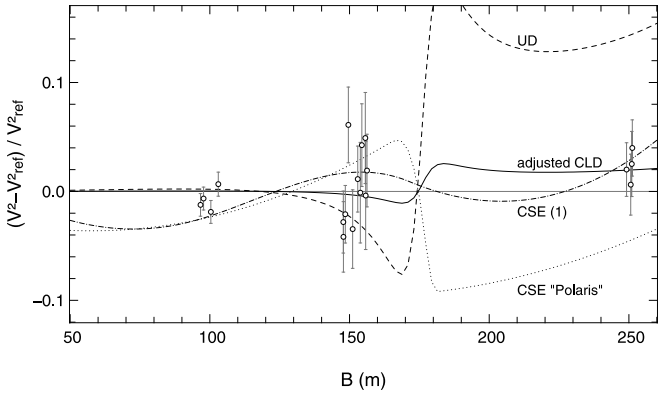

FIG. 7.—α Per squared visibility models: UD, adjusted CLD, PHOENIX, and two different CSE models are plotted here as the residuals to the PHOENIX CLD with respect to baseline. The common point at $B \approx 175$ m is the first minimum of the visibility function. The top of the second lobe is reached for $B \approx 230$ m. See Table 7 for parameters and reduced χ^2 of each model.

the angle between the stellar surface and the line of sight. The uniform disk diameter case corresponds to $\alpha = 0.0$, whereas an increasing value of α corresponds to a stronger CLD.

All visibility models for this work have been computed taking into account instrumental bandwidth smearing (Aufdenberg et al. 2006). From this two-parameter fit, we deduce a stellar diameter of $\theta_\alpha = 3.130 \pm 0.007$ mas and a power-law coefficient $\alpha = 0.119 \pm 0.016$. The fit yields a reduced $\chi^2 = 1.0$. There is a strong correlation between the diameter and CLD coefficient, 0.9. This is a well known effect, that a change in CLD induces a change in apparent diameter.

This fit is entirely satisfactory, as the reduced χ^2 is of order unity, and the residuals of the fit do not show any trend (Fig. 7). We note that this is not the case for Polaris (Paper II). Polaris, with u-v coverage very similar to α Per, does not follow a simple LD disk model, because it is surrounded by a faint CSE.

3.2.2. *Hydrostatic Models*

We computed a small grid of models, which consists of six one-dimensional, spherical, hydrostatic models using the PHOENIX general-purpose stellar and planetary atmosphere code version 13.11; for a description see Hauschildt et al. (1999) and Hauschildt & Baron (1999). The range of effective temperatures and surface gravities is based on a summary of α Per's parameters by Evans et al. (1996):

1. Effective temperatures, $T_{\rm eff} = 6150$, 6270, 6390 K.
2. $\log(g) = 1.4, 1.7$.
3. Radius, $R = 3.92 \times 10^{12}$ cm.
4. Depth-independent microturbulence, $\xi = 4.0$ km s^{-1}.
5. Mixing length to pressure scale ratio, 1.5.
6. Solar elemental abundance LTE atomic and molecular line blanketing, typically 10^6 atomic lines and 3×10^5 molecular lines dynamically selected at run time.
7. Non-LTE line blanketing of H I (30 levels, 435 bound-bound transitions), He I (19 levels, 171 bound-bound transitions), and He II (10 levels, 45 bound-bound transitions).
8. Boundary conditions: outer pressure 10^{-4} dynes cm^{-2}, extinction optical depth at 1.2 μm: outer was 10^{-10}, inner was 10^2.

For this grid of models the atmospheric structure is computed at 50 radial shells (depths), and the radiative transfer is computed along 50 rays tangent to these shells and 14 additional rays that impact the innermost shell, the so-called core-intersecting rays. The intersection of the rays with the outermost radial shell describes a center-to-limb intensity profile with 64 angular points.

TABLE 6
α PER PHOENIX MODELS

$T_{\rm eff}$ (K)	$\log g = 1.4$	$\log g = 1.7$
6150	0.137	0.136
6270	0.135	0.134
6390	0.133	0.132

NOTES.—Models tabulated for different effective temperatures and surface gravities. The K-band CLD is condensed into a power-law coefficient α: $I(\mu) \propto \mu^\alpha$.

Power-law fits to the hydrostatic model visibilities range from $\alpha = 0.132$ to 0.137 (Table 6), which correspond to 0.8–1.1 σ above the value we measured. Our measured CLD is below that predicted by the models, or in other words the predicted darkening is slightly overestimated.

3.3. *Possible Presence of CSE*

Firstly, we employ the CSE model used for Cepheids (Papers I and II). This model is purely geometrical, and it consists of a limb-darkened disk surrounded by a faint CSE, whose two-dimensional geometric projection (on the sky) is modeled by a ring. The ring parameters consist of the angular diameter, width, and flux ratio with respect to the star ($F_s/F_\star$). We adopt the same geometry found for Cepheids: a ring with a diameter equal to 2.6 times the stellar diameter (Paper II) with no dependency with respect to the width (fixed to a small fraction of the CSE angular diameter, say 1/5).

This model restriction is justified because testing the agreement between a generic CSE model and interferometric data requires a complete angular resolution coverage, from very short to very large baselines. Although our α Per data set is diverse regarding the baseline coverage, we lack a very short baseline ($B \sim 50$ m), which was not available at that time at the CHARA Array.

The simplest fit consists in adjusting the geometrical scale; the angular size ratio between the CSE and the star is fixed. This yields a reduced χ^2 of 3, than at 1.1 for a hydrostatic LD and 1.0 for an adjusted CLD law (Table 7).

We can force the data to fit a CSE model by relaxing the CLD of the star or the CSE flux ratio. A fit of the size of the star and the brightness of the CSE leads to a reduced χ^2 of 1.4 and results in a

TABLE 7
MODELS FOR α PER

Model	$\theta_\star$ (mas)	α	$F_s/F_\star$ (%)	χ^2_r
UD	3.080 ± 0.004	0.000	...	5.9
PHOENIX CLD	3.137 ± 0.004	0.135	...	1.1
adjusted CLD	3.130 ± 0.007	0.119 ± 0.016	...	1.0
CSE "Polaris"	3.086 ± 0.007	0.135	1.5	3.0
CSE (1)	3.048 ± 0.007	0.066 ± 0.004	1.5	1.4
CSE (2)	3.095 ± 0.010	0.135	0.06 ± 0.26	1.4

NOTES.—The parameters are: $\theta_\star$ is the stellar angular diameter, the CLD power-law coefficient is α, and if relevant, the brightness ratio between the CSE and the star is $F_s/F_\star$. The first line is the uniform disk diameter, the second one is expected CLD from the PHOENIX model, and the third one is the adjusted CLD. The fourth line is a scaled Polaris CSE model (Paper II). The last two lines are attempts to force a CSE model to the data. Lower script are uncertainties, the absence of lower script means that the parameter is fixed.

TABLE 8
Relative Flux in K Band for the CSE Discovered around Cepheids and the Nonpulsating α Per

Star	Period (days)	CSE Flux (%)
α UMi	3.97	1.5 ± 0.4
δ Cep	5.37	1.5 ± 0.4
Y Oph	17.13	5.0 ± 2.0
ℓ Car	35.55	4.2 ± 0.2
α Per	...	<0.26

very small flux ratio between the CSE and the star of 0.0006 ± 0.0026, which provides an upper limit for the CSE flux of 0.26% (compared to 1.5% for Polaris and δ Cep for example, and 5% for Y Oph). On the other hand, forcing the flux ratio to match that for Cepheids with CSEs and leaving the CLD free leads to a reduced χ^2 of 1.4 but also to a highly unrealistic $\alpha = 0.066 \pm 0.004$ (Table 7 and Fig. 7).

This leads to the conclusion that the presence of a CSE around α Per similar to the measured Cepheid CSE is highly improbable. As shown above, the measured CLD is slightly weaker ($1\ \sigma$) than one predicted by model atmospheres. A compatible CSE model exists if the CLD is actually even weaker but in unrealistic proportions.

3.4. *Conclusion*

The observed α Per visibilities are not compatible with the presence of a CSE similar to those detected around Cepheids. The data are well explained by an adjusted center-to-limb darkening. The strength of this CLD is compatible with the hydrostatic model within $1\ \sigma$.

4. DISCUSSION

Using the interferometric Baade-Wesselink method, we determined the distance to the low-amplitude Cepheid Y Oph to be $d = 491 \pm 18$ pc. This distance has been unbiased from the presence of the circumstellar envelope. This bias was found to be of the order of 4% for our particular angular resolution and the amount of CSE we measured. Y Oph's average linear diameter has also been estimated to be $R = 67.8 \pm 2.5\ R_\odot$. This latter quantity is intrinsically unbiased by either the center-to-limb darkening or the presence of a circumstellar envelope. This value is found to be substantially lower, almost $4\ \sigma$, than the period-radius relation prediction $R = 100 \pm 8\ R_\odot$. Among other peculiarities, we found a very large phase shift between radial velocity measurements and interferometric measurements: $\Delta\phi = -0.074 \pm 0.005$, which corresponds to more than 1 day. For these reasons, we think Y Oph should be excluded from future calibrations of popular relations for classical Cepheids, such as the period-radius and period-luminosity relations.

So far, the four Cepheids we looked at have a CSE: ℓ Car (Paper I), Polaris, δ Cep (Paper II), and Y Oph (this work). On the other hand, we have presented here similar observations of α Per, a nonpulsating supergiant inside the instability strip, which provides no evidence for a circumstellar envelope. This nondetection reinforces the confidence we have in our CSE detection technique and draws more attention to a pulsation-driven mass-loss mechanism.

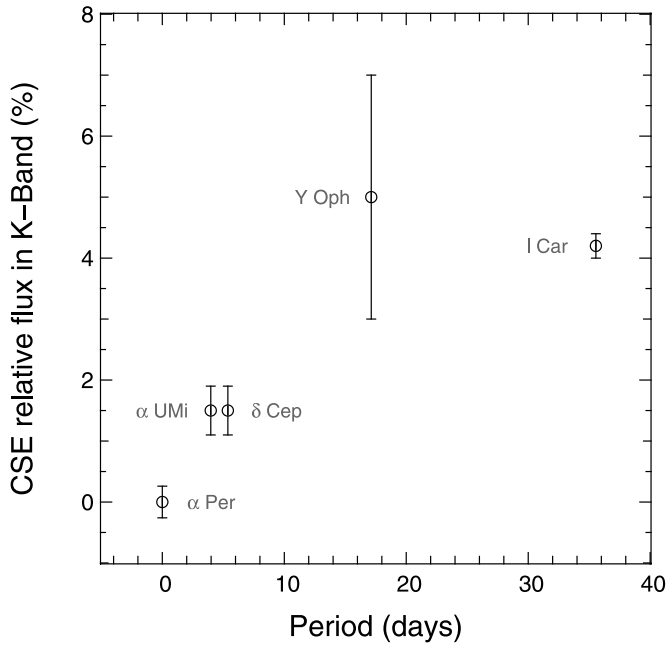

Fig. 8.—Measured relative K-band CSE fluxes (*in percent*) around Cepheids as a function of the pulsation period (*in days*). The nonpulsating yellow supergiant α Per is plotted with $P = 0$.

Interestingly, there seems to be a correlation between the period and the CSE flux ratio in the K band: short-period Cepheids seem to have a fainter CSE compared to longer period Cepheids (Table 8 and Fig. 8). Cepheids with long periods have higher masses and larger radii; thus, if we assume that the CSE K-band brightness is an indicator of the mass-loss rate, this would mean that heavier stars experience higher mass-loss rates. This is of prime importance in the context of calibrating relations between Cepheids' fundamental parameters with respect to their pulsation periods. If CSEs have some effects on the observational estimation of these fundamental parameters (luminosity, mass, radius, etc.), a correlation between the period and the relative flux of the CSE can lead to a biased calibration.

Research conducted at the CHARA Array is supported at Georgia State University by the offices of the Dean of the College of Arts and Sciences and the Vice President for Research. Additional support for this work has been provided by the National Science Foundation through grants AST 03-07562 and 06-06958. We also wish to acknowledge the support received from the W. M. Keck Foundation. This research has made use of SIMBAD database and the VizieR catalogue access tool, operated at CDS, Strasbourg, France.

REFERENCES

Aufdenberg, J. P., et al. 2006, ApJ, 645, 664
Barnes, T. G., III, Storm, J., Jefferys, W. H., Gieren, W. P., & Fouqué, P. 2005, ApJ, 631, 572
Butler, R. P. 1998, ApJ, 494, 342
Coude Du Foresto, V., Ridgway, S., & Mariotti, J.-M. 1997, A&AS, 121, 379
Evans, N. R., Teays, T. J., Taylor, L. L., Lester, J. B., & Hindsley, R. B. 1996, AJ, 111, 2099
Fernie, J. D., Evans, N. R., Beattie, B., & Seager, S. 1995a, Inf. Bull. Variable Stars, 4148, 1
Fernie, J. D., Khoshnevissan, M. H., & Seager, S. 1995b, AJ, 110, 1326

Gorynya, N. A., Samus', N. N., Sachkov, M. E., Rastorguev, A. S., Glushkova, E. V., & Antipin, S. V. 1998, Astron. Lett., 24, 815
Hatzes, A. P., & Cochran, W. D. 2000, AJ, 120, 979
Hauschildt, P. H., Allard, F., Ferguson, J., Baron, E., & Alexander, D. R. 1999, ApJ, 525, 871
Hauschildt, P. H., & Baron, E. 1999, J. Comp. Applied Math., 109, 41
Heiles, C. 2000, AJ, 119, 923
Hestroffer, D. 1997, A&A, 327, 199
Kervella, P., Mérand, A., Perrin, G., & Coudé Du Foresto, V. 2006, A&A, 448, 623 (Paper I)
Kervella, P., Nardetto, N., Bersier, D., Mourard, D., & Coudé du Foresto, V. 2004a, A&A, 416, 941
Kervella, P., Thévenin, F., Di Folco, E., & Ségransan, D. 2004b, A&A, 426, 297
Kholopov, P. N., et al. 1998, Combined General Catalogue of Variable Stars (ver. 4.1; Moscow: Sternberg Astron. Inst.)
Lane, B. F., Kuchner, M. J., Boden, A. F., Creech-Eakman, M., & Kulkarni, S. R. 2000, Nature, 407, 485
Marengo, M., Karovska, M., Sasselov, D. D., Papaliolios, C., Armstrong, J. T., & Nordgren, T. E. 2003, ApJ, 589, 968
Marengo, M., Karovska, M., Sasselov, D. D., & Sanchez, M. 2004, ApJ, 603, 285
Mérand, A., Bordé, P., & Coudé Du Foresto, V. 2005a, A&A, 433, 1155
Mérand, A., Coudé du Foresto, V., Kellerer, A., ten Brummelaar, T., Reess, J.-M., & Ziegler, D. 2006a, in Advances in Stellar Interferometry, ed. J. D. Monnier, M. Schöller, & W. C. Danchi, Proc. SPIE, 6268, 62681F
Mérand, A., et al. 2005b, A&A, 438, L9
———. 2006b, A&A, 453, 155 (Paper II)
Moskalik, P., & Gorynya, N. A. 2005, Acta Astron., 55, 247
Nardetto, N., Fokin, A., Mourard, D., Mathias, P., Kervella, P., & Bersier, D. 2004, A&A, 428, 131
Nordgren, T. E., Sudol, J. J., & Mozurkewich, D. 2001, AJ, 122, 2707
ten Brummelaar, T. A., et al. 2005, ApJ, 628, 453
Turner, D. G., Abdel-Sabour Abdel-Latif, M., & Berdnikov, L. N. 2006, PASP, 118, 410
Vinko, J., Remage Evans, N., Kiss, L. L., & Szabados, L. 1998, MNRAS, 296, 824